Silicon (2024) 16:3461–3470
https://doi.org/10.1007/s12633-024-02940-x

RESEARCH

Design of a High Efficiency p-Si Based Heterojunction Solar Cell with In_2S_3 Window and NiO BSF Layers

Nusrat Jahan Konok[1] · Shaikh Khaled Mostaque[1] · Jaker Hossain[1]

Received: 6 December 2023 / Accepted: 2 March 2024 / Published online: 7 March 2024

Abstract

The numerical evaluation performed on the design of n-In_2S_3/p-Si/p^+-NiO solar cell reveals that it can come up with a high efficiency gain along with substantial values in other photovoltaic parameters. The pristine n-In_2S_3/p-Si structure imparts a power conversion efficiency, PCE of 23.24%. The selection of NiO in back surface field (BSF) layer makes an improvement of ~ 0.1 V in open circuit voltage, V_{OC} and a slight improvement in short circuit current density, J_{SC}. Under single sun and AM 1.5G spectrum, the optimum thickness (Window = 0.2 µm, Base = 350 µm, BSF = 0.2 µm), doping concentration ($Window_{donor} = 1.0 \times 10^{18}$ cm^{-3}, $Base_{acceptor} = 1.0 \times 10^{17}$ cm^{-3}, $BSF_{acceptor} = 1.0 \times 10^{20}$ cm^{-3}) and defect density (Window = 1.0×10^{14} cm^{-3}, Base = 1.0×10^{12} cm^{-3}, BSF = 1.0×10^{14} cm^{-3}) provide an enhanced PCE of 26.74% with the application of NiO as BSF in the pristine structure. The other photovoltaic parameters results with $V_{OC} = 0.79$ V, $J_{SC} = 40.37$ mA/cm^2 and FF = 83.85%. Insertion of a thin and optimized NiO reduces recombination at the back surface by a potential barrier that enhances V_{OC} and current in the device. Such a cost-effective solar cell exhibits enough possibility of fabricating a highly efficient, reliable and promising performance device.

Keywords p-Silicon · In_2S_3 window · NiO BSF · High efficiency · SCAPS-1D

1 Introduction

P-type (p-Si) based solar cells have received a lot of interest due to their to substantial accessibility, lower cost [1]. In application field they are frequent in space technologies and have proven to be resilient to radiation [2]. Their cell operation mainly involves: (i) absorption of sunlight and corresponding generation of electron–hole pair, (ii) separation of charge carriers at the terminals and (iii) external circuit capable of collecting the carriers [2, 3]. Such a cell considering an infinite number of connections and extremely focused sunlight can achieve a limiting efficiency of 86.8% [4, 5]. In today's marketplace, a variety of tandem, two-layer or multilayered cells are frequently offered with ~ 30% efficiency under one-sun illumination. For instance, a recent work with the application of methyl ammonium tin mixed halide based materials in different layers of a Si-based tandem solar cell displays 30.7% PCE with high V_{OC} of 2.14 V [6]. Such performance can be improved to nearly 40% under centralized rays, but it may rise the overall complexity and the manufacturing costs [7, 8].

In an effort to find a fantastic answer to the problem at hand, various combinations of window, base and back surface materials have been sought in some recent works and the end result is always a lightweight and uncomplicated construction approach [9–11]. In the similar pattern, we propose a solar cell with three different materials namely silicon, indium sulphide (In_2S_3) and nickel oxide (NiO) which can form two heterojunctions and theoretically comes up with high standard of exemplary cell performance.

The bandgap value of Si ($E_g = 1.12$ eV and corresponding wavelength for light absorption $\lambda_{cut\text{-}off} = 1107$ nm) are extremely close to the ideal values for single absorber solar-to-electric energy conversion. The amount of light that is coupled into the silicon absorber can be maximized by reducing losses due to parasitic absorption and surface reflection regardless of the stacking or deposition method [12].

With thin film technology, the bandgap of In_2S_3 has been found to vary between 2.0–3.7 eV providing high

✉ Jaker Hossain
jak_apee@ru.ac.bd

[1] Solar Energy Laboratory, Department of Electrical and Electronic Engineering, University of Rajshahi, Rajshahi 6205, Bangladesh

transmittance between 380 to 700 nm. In comparison with popular CdS in window, In_2S_3 is nontoxic and comes up with high stability and high carrier mobility [13]. Moreover, good transparency and photoconductive ability of In_2S_3 has made it an alternative candidate to replace CdS window [14]. Some diverse in-line processing techniques for deposition of In_2S_3 thin films such as thermal evaporation, chemical bath deposition, physical vapor deposition, atomic layer deposition, successive physical layer adsorption and reaction, pyrolysis etc. are commonly recognized [13, 15, 16]. Likewise, NiO thin film can also be deposited using varieties of methods like pulsed laser deposition, e-beam technique, chemical vapour deposition, sputtering or even spin coating and inkjet printing [17]. It is possible to tailor some properties of the NiO thin films with annealing or plasma treatment. Additionally, a wide variety of tunings of work function from 3.7 to 6.7 eV, can be achieved by varying the surface dipole, composition, or defect density [18].

Effects like surface recombination will become more prominent as the p-type monocrystalline wafer gets thinner. Hence, measures to control or lessen this effect are ought to be taken. One way to reduce back surface recombination in a p-type wafer is to apply BSF layer with the base structure [19, 20].

Previously, NiO has demonstrated its capacity to significantly reduce carrier recombination at the contacts when used as a BSF with CdTe based cells, leading to improved V_{OC} [21]. By several research groups, NiO has been successfully found to be employed as hole transport layer in CdTe and SnS based cells along with some perovskite structures [22–24]. Non-stoichiometric oxygen-rich NiO films develop into reasonably excellent p-semiconductors with wide band gap of 3.7 eV. Properties like exceptional chemical stability, low cost, and magnetic, electric, and optical properties of NiO films have made them a desirable p-type oxide semiconductor for use in optoelectronic applications [25]. The recombination at the back of solar cells becomes an issue and can directly lower efficiency when charge carriers are slightly out of the field. Studies reveal that the addition of NiO causes increment of potential barrier at the back contact along with reduction of recombination with higher V_{OC}. Therefore, we suggest the formation of heavily doped p^+-NiO at the back surface of p-Si centric bulk Si, enabling efficient separation of hole and electron at the back which in turn can reduce their recombination and can increase total quantum efficiency. Thick NiO can lead to a dominant potential barrier causing deteoriation in the cell performance [26]. To overcome such complexities, the thickness as well as other parameters like doping concentration and defect density have been optimized here as suggested by the previous studies [27]. To the best of our knowledge, such possibility of In_2S_3 and NiO has never been studied with silicon before.

In this work, we propose n-In_2S_3/p-Si/p^+-NiO-based double-junction structure where we perform numerical simulations for obtaining band diagram, J-V charachteristics, quantum Efficiency, optimization of associated layers and observing other features related to solar cell. The standard AM 1.5G global spectrum has been utilized throughout the simulations to identify overall performance parameters.

2 Device Architecture and Calculation

Figure 1 represents the structured layout of the propounded Si solar cell along with its illuminated energy band diagram. Incident photons from sun first fall on to n-type thinner window and reaches to the n/p window-absorber junction as shown in Fig. 1(a). It is evident that p-Si makes a satisfactory band alignment with n-In_2S_3 window as well as p^+-NiO BSF layer as illustrated in Fig. 1(b). The changes in photovoltaic characteristics i.e. V_{OC}, J_{SC}, FF and PCE with optimized values have been discussed later with this work.

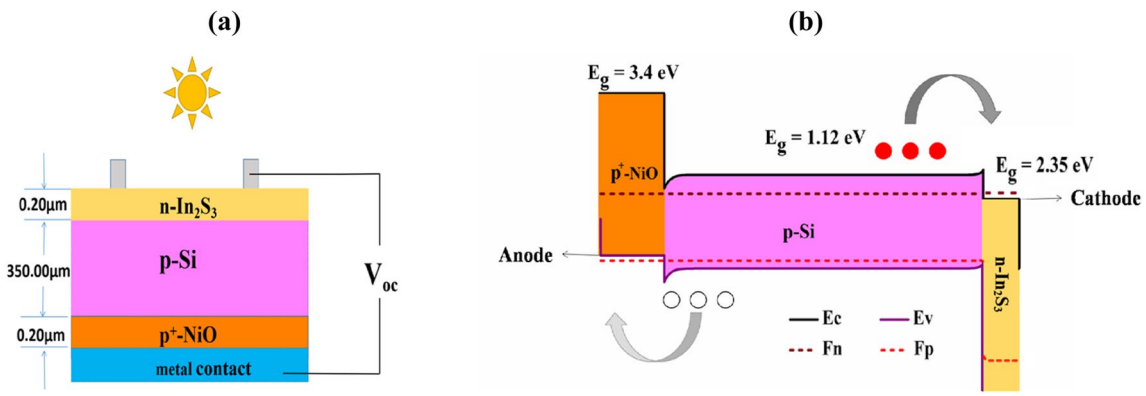

Fig. 1 **a** Proposed p-Si centric solar cell showing layer optimized thickness and **b** its energy band diagram (not to scale) when lit with AM 1.5G solar spectrum

The simulation software SCAPS-1D (version 3.3.07) has been exerted to calculate solar device outcomes [11, 23]. The absorption interpolation model for In_2S_3 and NiO have been chosen from traditional model of the simulator. The absorption profile for p-Si has been selected from SCAPS default files. Rest of the parameters required for simulation have been selected from previous reports and are included in Table 1 [24, 28, 29]. With such parameters, the bending of the energy band at junctions have been happened in such a way that an easy path has been created for electron to be collected by Ti metal grid above the window layer. On the contrary, the proper collection of holes has been ensured by the BSF with E_V values above the Si layer. E_V indicates the energy of valence band while F_n and F_p denote the Fermi energy levels for electron and hole, in turn. The energy level of F_p lies below the E_V of NiO and goes inside the energy band gap of In_2S_3. Likewise, F_n energy level goes over by a small amount of conduction level energy E_C of In_2S_3 and passes between NiO energy bandgap. Note that, the E_C and E_V values are at 1.37 and -0.97 eV, respectively at In_2S_3 layer that contains a bandgap of 2.35 eV and electron affinity of 4.40 eV [30]. In the rear field, NiO has the electron affinity of 1.45 eV with a bandgap of 3.4 eV creating E_C and E_V values at 2.28 and 5.37 eV, respectively [31]. Thus, they create proper dual heterojunctions with Si containing the bandgap of 1.12 eV and electron affinity of 4.05 eV.

Moreover, the following values in Table 2 have been also considered in each layer. In all levels, Gaussian energetic distribution with reference for defect energy above $E_V(< 2.7)$, energy level with respect to reference 0.35 eV with characteristic energy of 0.10 eV have been considered.

Table 2 Constant properties considered in proposed p-Si solar cell

Parameters	Value
Electron and hole thermal velocity (cm/s)	1.0×10^{7}
Electron capture cross section (cm^2)	1.0×10^{-15}
Hole capture cross section (cm^2)	1.0×10^{-17}
Temperature (K)	300
Incident(or bias) light power (W/m^2)	1000
Transmission(%)	100

3 Results and Discussion

3.1 J-V Characteristics and QE Performance of the Proposed Model

Figure 2(a) signifies the J-V characteristics of the proposed cell along with its photon absorption performance corresponds to wavelength between 300–1400 nm. The pristine structure with single n^+/p junction cell exhibits 0.72 V of V_{OC} and 38.12 mA/cm^2 of J_{SC} with corresponding FF of 84.75% and resultant PCE of 23.24%. On the contrary, the addition of only 0.2 µm thick NiO in optimized condition provides an improvement in V_{OC} as well as a marginal rise in $J_{SC.}$ The addition of NiO ($E_g = 3.4$ eV) creates a proper heterojunction with Si ($E_g = 1.12$ eV) and thereby the double heterojunction of $n/p/p^+$ in the proposed structure provides an enhanced V_{OC} of 0.79 V. The suppression of carrier recombinations at the surface owing to the diminishing of speed of surface recombination by the electric field of Si/NiO interface escalates both the V_{OC} and J_{SC} of the silicon device and exalted the PCE to 26.74% [10, 11, 24].

The QE graph illustrated in Fig. 2(b) further explains corresponding absorption of photons due to addition of NiO

Table 1 Properties of different layers in the p-Si solar cell structure

Parameters	n-In_2S_3	p-Si	p^+-NiO
Thickness (µm)	0.20	350.00	0.20
Bandgap, E_g (eV)	2.35	1.12	3.40
Electron affinity (eV)	4.40	4.05	1.45
Dielectric permittivity (relative)	13.50	11.90	10.07
CB effective density of states ($1/cm^3$)	2.20×10^{17}	1.05×10^{19}	2.80×10^{19}
VB effective density of states ($1/cm^3$)	1.80×10^{19}	3.92×10^{18}	1.00×10^{19}
Electron mobility (cm^2/Vs)	1.0×10^{2}	3.9×10^{3}	1.2×10^{1}
Hole mobility (cm^2/Vs)	2.5×10^{1}	1.9×10^{3}	2.8×10^{0}
Shallow uniform donor density, N_D ($1/cm^3$)	1.0×10^{18}	0.00	0.00
Shallow uniform acceptor density, N_A ($1/cm^3$)	0.00	1.0×10^{17}	1.0×10^{20}
Density of defects (cm^{-3}) (above E_v w.r.t. E_{ref} (eV))	1.0×10^{14}	1.0×10^{12}	1.0×10^{14}
Type of defects	Single acceptor	Single donor	Single donor
Energetic distribution	Gaussian	Gaussian	Gaussian
Energy level with respect to Reference (eV)	1.91	0.35	0.65

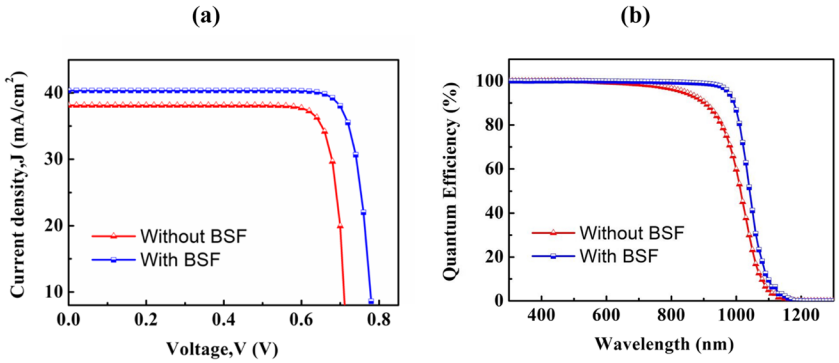

Fig. 2 The (**a**) J-V characteristic curves and (**b**) Quantum efficiency in the proposed optimized Si solar cell

with this regard. According to the QE, all photons with comparable wavelengths less than 1200 nm have been absorbed. It indicates that the entire wavelength has been absorbed by the p-Si base. Figure 2(b) makes evident how the NiO facilitates the extra electron–hole (e–h) separation generated by the photons of slightly longer wavelengths in Si absorber. For comparison, the QE for the pristine structure is ~ 72% in the wavelength of 970 nm while the proposed model still displays QE of ~ 96%. In 1050 nm, the QE of pristine structure falls to ~ 23% and the addition of BSF provides the advantage of having QE of ~ 46%. In light of this, it is evident that a NiO BSF even with a small thickness can prevent minority carriers from entering the recombination surface, which in turn contributes to the upsurge and persistence of the V_{OC} and J_{SC} [20]. Some previous studies with dual heterojunctions also come up with an intensification of this voltage [28, 32–35]. As the bandgap of NiO is a bit higher than that of p-Si, it creates well prevention to the minority carrier progression which in turn reduces surface recombination velocity [10, 11, 24]. As a result, J_{SC} gets enhanced nearly about 2.25 mA/cm^2 and displays a J_{SC} of 40.37 mA/cm^2 in the proposed structure [36]. Thus, the amelioration of both V_{OC} and J_{SC} with the establishment of n-ln_2S_3/p-Si/p^+-NiO causes overall PCE to improve about 3.5% and culminate in 26.74%.

3.2 Consequences of Changes in Operating Temperature

Like the most of the semiconductor devices, the proposed Si solar cell has been modeled at an operating temperature of 300 K. The changes in the temperature follows the conventional cell output pattern as shown in Fig. 3. From previous reports, it is usual for Si based cell that the rise in temperature decreases V_{OC} and slightly elevates J_{SC} [37–39]. From the general expression of V_{OC}, we know,

$$V_{OC} = V_{th}.\ln\left(\frac{J_{SC}}{J_o} + 1\right) \tag{1}$$

The reliance of V_{OC} on temperature can be explained from the following equation for the temperature range of 273–523 K in p-Si [38].

$$\frac{dV_{OC}}{dT} = \frac{V_{OC}}{T} + V_{th}\frac{1}{J_{SC}}\frac{dJ_{SC}}{dT} - \left(\frac{E_g(0)}{T} + \frac{\alpha T}{(T+\beta)^2}\right) \tag{2}$$

Here, J_o represents reverse saturation current density, $E_g(0) = E_g$ indicates bandgap at $T = OK$ with T being the absolute

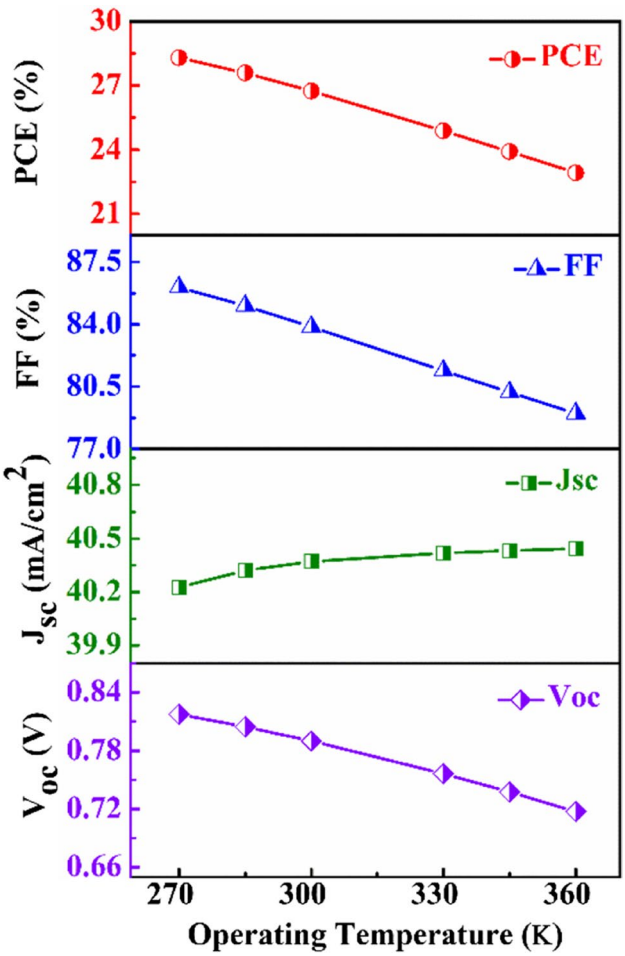

Fig. 3 The effect of variation in operating temperature on proposed cell parameters

temperature and α, β are two empirical parameters. $V_{th} = kT/q$ defines the thermal voltage, where k is the Boltzmann's constant and q represents the electron charge. Thus, the variation of temperature ranging from 270–360 K causes a decrement of V_{OC} from 0.81 V to 0.71 V in the proposed structure. In the same range, we also see a small enhancement of current from 40.22 to 40.44 mA/cm^2 attributed to the fact of capturing more photons leading by a shrunk in bandgap [38]. Moreover, the Fermi–Dirac distribution can represent how carriers populate energy levels [40]. As the bandgap decreases with thermal energy, the J_{SC} slightly increases the as the photon cut-off wavelength shifts to a longer wavelength of the spectrum enabling creation of more e–h pairs. However, such a change for J_{SC} is very small compared to the change in V_{OC} [41]. As the change in V_{OC} dominates, FF and corresponding PCE follows the similar pattern [38]. Thus, FF shows a decrement from 86.07 to 79% and corresponding PCE suffers a fall of 28.3 to 22.92% for the proposed structure.

3.3 Series and Shunt Resistance's Impact on the Proposed Model

Though the optimized structure has been experimented without any parasitic parameters namely series and shunt resistances, the effect of their addition has been delineated in Fig. 4. In reality, it is natural for a cell to show certain series resistance originating from the lump and contacts. In contrast, leakage current forming fabrication defects drive the shunt resistance [10]. In general, low values of series and higher values of shunt resistances of the devices must be achieved in order to design and construct efficient PV devices [42]. From Fig. 4(a), we hardly find any effect on V_{OC} and J_{SC} due to change in series resistance from 0 to 5 Ω.cm^2. However, like previous findings, FF drastically falls from 83.35 to 60.8% due to change in 5 Ω.cm^2 which in turn takes the value of PCE down to 19.4% [10, 42].

Shunt resistance also has a considerable effect on the observed output as depicted in Fig. 4(b). With shunt resistance starting from the lower order of ten, V_{OC} advances until it touches its maximum value at 0.79 V. Considering zero shunt the device results the J_{SC} of 40.37 mA/cm^2. J_{SC} remains on the same value as expected from the general theoretical expressions of Si solar cell. Consequently, FF follows the changes of V_{OC}. At the order of 10^2 Ω.cm^2, V_{OC} gets raised at 0.78 V with FF of 70.02%. In the higher order of shunts, we find gradual rise of FF to 83.84% as V_{OC} reaches at 0.79 V and the corresponding PCE displays the optimized value of 26.74%.

3.4 Optimization of Window, Absorber and BSF Layer in the Proposed Model

The simulation has been run with variation of three parameters namely thickness, carrier and defect density in each part to find the highest PCE with considerable amount of V_{OC}, J_{SC} and FF. The simulations result three figures in each layer while keeping the values of corresponding layers in optimum condition. The outputs give an indication on how the device performance may vary during fabrication of real time cells. However, the ultimate target is to find the theoretical optimized condition that gives the highest PCE.

Figure 5(a), (b) and (c) display the consequences of changes in the parameters of In_2S_3 window layer. The

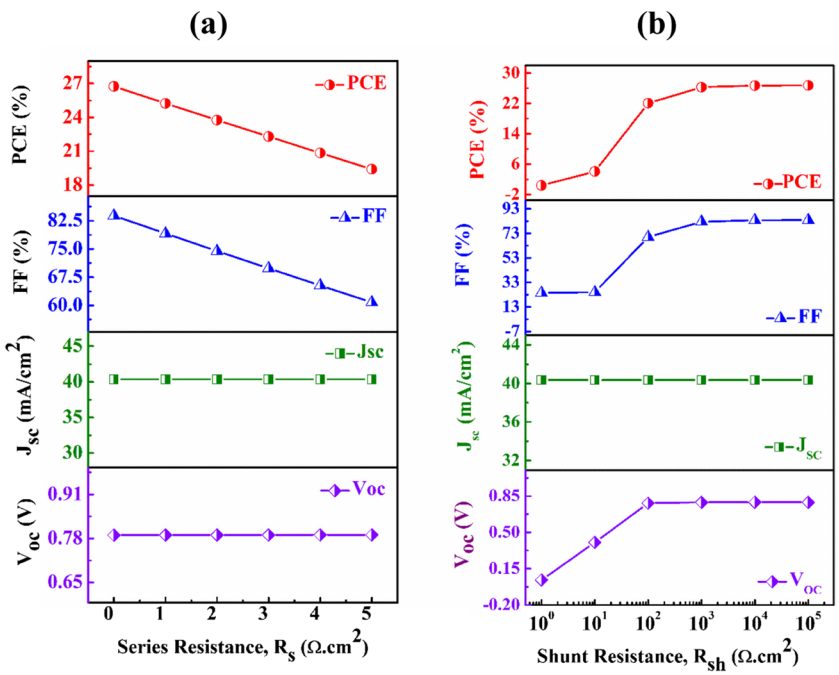

Fig. 4 **a** The remifications of changing series and (**b**) shunt resistance to the proposed structure

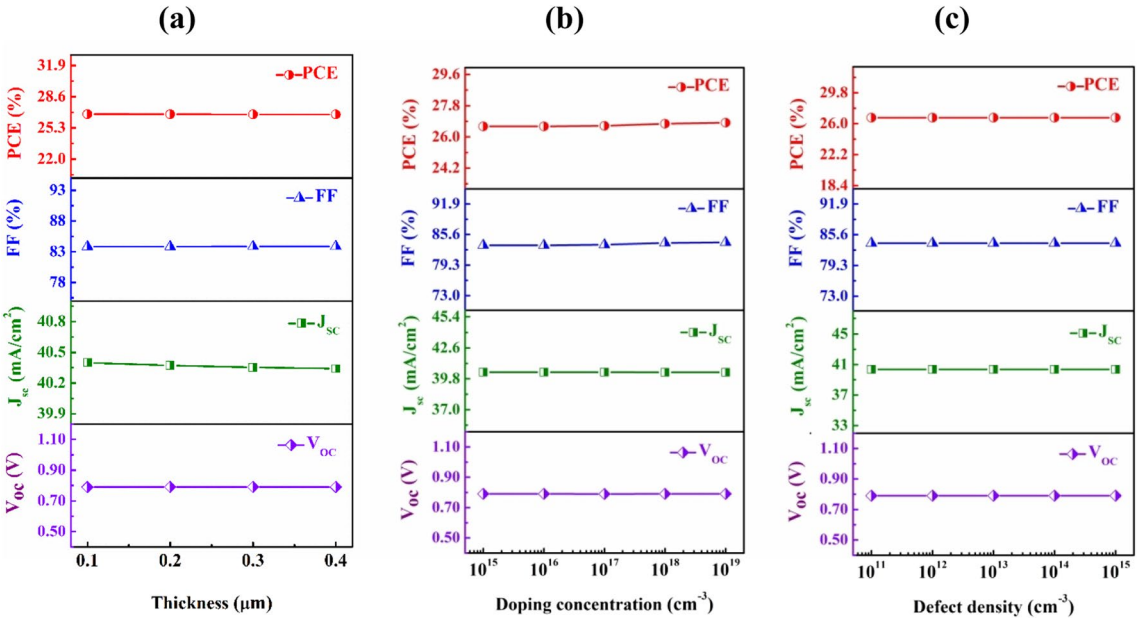

Fig. 5 **a** Thickness, **b** carrier and **c** defect density variation in In_2S_3 window layer of proposed Si solar cell

disparity in thickness, doping concentration or defect density in the window does not seem to make a significant effect in the operation of the propound structure. Here, the breadth of window layer has been deviated between 0.1 and 0.4 μm while the doping concertation and defect densities have been varied between the ranges from 10^{15} to 10^{19} cm^{-3} and 10^{11} to 10^{15} cm^{-3}, respectively. As In_2S_3 possess wide bandgap of 2.35 eV, a trivial fluctuation occurs in the investigated range of thickness. Even the alteration in other parameters does not seem to affect the cell performance at all [34, 43]. Thus, the optimum width and carrier concentration have been chosen at 0.2 μm and 10^{18} cm^{-3}, respectively with considerable defect density of 10^{14} cm^{-3}.

In Fig. 6, we observe the cell performance due to the similar variation of parameters in *p*-Si layer. The addition of 300 μm absorber width does not create a notable change in output as illustrated in Fig. 6(a). However, the addendum of thickness provides the opportunity of greater absorption

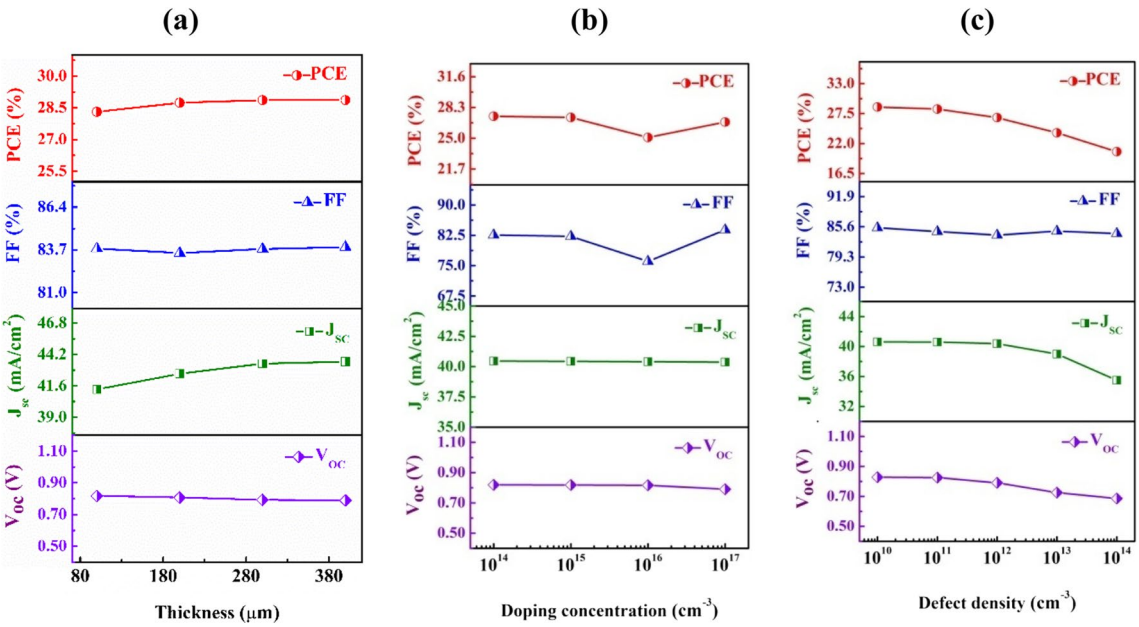

Fig. 6 **a** Thickness, **b** doping and **c** defects variation in *p*-Si absorber of proposed solar cell

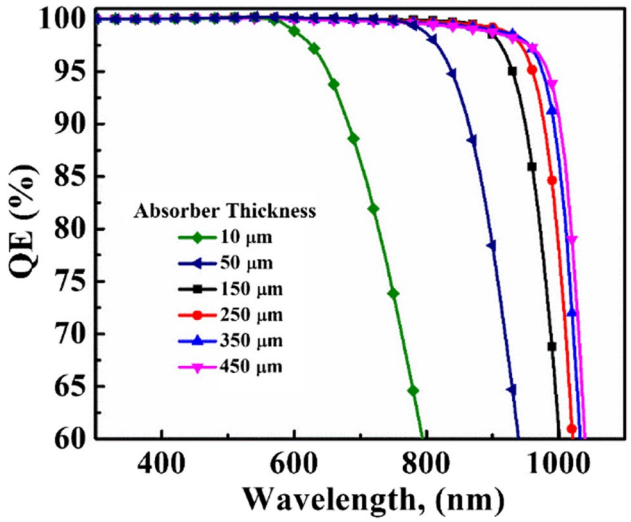

Fig. 7 Variation of QE for different p-Si thickness in the proposed structure

of photons than before [34, 44]. As a consequence, we see a gradual increment in the values of J_{SC}. At 350 µm of thickness the V_{OC} results with 0.79 V and J_{SC} comes with 43.43 mA/cm^2. These values provide an acceptable FF of 83.76% and PCE with 28.86% which tend to rise with further addition.

There are no significant variations in V_{OC} and J_{SC} with addendum of higher order of carriers from 10^{14} cm^{-3} to 10^{17} cm^{-3} as delimitates in Fig. 6(b). FF drops down to 76.06% at 10^{16} cm^{-3} which is 82.59% at 10^{14} cm^{-3}. This reduction can be explained by a declining ratio between the rates of charge carrier production and recombination in the p-Si layer [45]. At higher acceptor densities, in the order of 10^{18} cm^{-3}, the FF again rises to 83.85%. This is attributed to a rise in the electric field (Schottky barrier) close to NiO, as well as an increase in the creation and recombination rates of free charges [45]. Furthermore, FF also gets improved with the small value of series resistance and a drop of diode ideality factor at higher acceptor densities [11, 46]. The efficiency seems to follow the FF pattern and at 10^{17} cm^{-3} the optimum efficiency is found to be 26.74% with FF of 83.85%.

It seems obvious that, the cell performance gets degraded with the addition of defect density in the absorber layer. It is seen from the Fig. 6(c) that V_{OC} faces a detrimental performance with the incremental order of defect densities. At the order of 10^{10} cm^{-3}, the PCE comes with 28.72% with voltage of 0.82 V and current of 40.61 mA/cm^2. These values get lowered as the order is changed to 10^{14} cm^{-3} and result the voltage of 0.68 V with photocurrent of 35.51 mA/cm^2 and PCE of 20.52%. The SRH carrier recombination mechanism plays the principal role at higher order of defect densities. It causes recombination of carriers which in turn stimulates the dark current and lowers corresponding V_{OC} as well as the J_{SC} [34, 43, 47]. With the above findings we choose 350 µm thick p-Si absorber to be doped in the concentration order of 10^{17} cm^{-3} while maintaining the defect in the order of 10^{12} cm^{-3} to achieve the highest PCE.

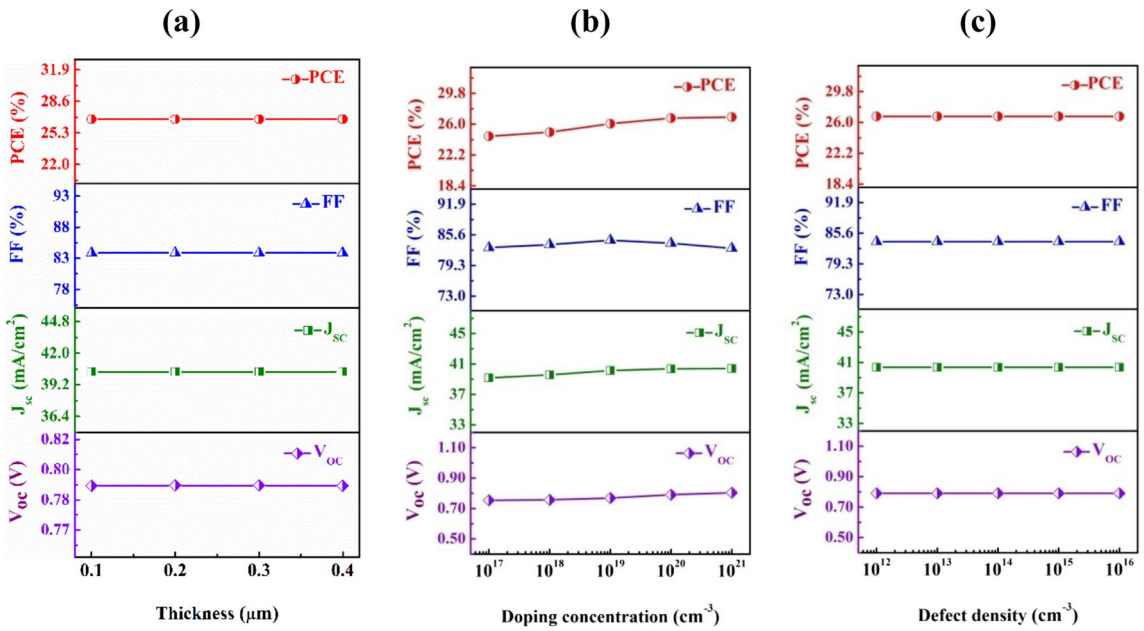

Fig. 8 **a** Thickness, **b** doping and **c** defect density variation in NiO BSF layer of proposed solar cell

Figure 7 illustrates the QE variation over the p-Si thickness ranging from 10 to 450 µm. It is inferred that, with the addition of absorber thickness, the longer wavelength photons take part in generation of additional e–h pairs [6, 45]. For instance, the QE related to 10 µm of Si thickness drops to 60% correspond to incident photon wavelength of 790 nm. Increasing the thickness to 50 µm achieves QE of 99% for same wavelength of photons and similar drop occurs at wavelength of around 940 nm. This is happened as at least a width of 30 µm for silicon is needed to absorb photons of wavelength upto 900 nm [48]. When the layer is too thick, photo generated carriers must travel a larger distance to window and BSF for collection of carriers and a significant loss can occur [45]. QE does not show any major enhancement after the increment of absorber thickness over 400 µm.

The width of NiO BSF layer, doping concentration and defect densities have been varied and the corresponding outcomes are delineated in Fig. 8. All the figures show that the alteration in thickness, doping and defects of NiO has negligible effect on the operation of the Si solar cell. The results are similar to the results of some previous works [10, 29]. The V_{OC} is almost constant at 0.79 V with thickness but has got a slight increment along with doping. The J_{SC} also remains constant at 40.37 mA/cm^2 which might have faced a slight improvement with increment in doping orders. Such increment may come with the possible enhancement in the carrier dependent lifetime along with the surface recombination speed and the reduction in excess minority carriers with relative high potential in $n^+/p/p^+$ interface [49]. The defects in the studied range do not tend to cause any declination in cell performance as the carrier diffusion length is high enough compared to the width of the BSF that can rise recombination current in the device [9, 10]. Therefore, we have chosen an optimum thickness of NiO of 0.2 µm with a doping of 10^{20} cm^{-3} with defects of 10^{14} cm^{-3}.

4 Conclusions

In this work, the performance of a p-Si based cell with n-In_2S_3 window has been analyzed with and without the addition of NiO BSF layer. The band diagram of n-In_2S_3/p-Si/p^+-NiO solar cell reveals the perfect alignment of each layer. The proposed design comes with a PCE of 26.74% with V_{OC} = 0.79 V, J_{SC} = 40.370 mA/cm^2 and FF = 83.85%. The optimized thickness and doping density of Si are 350 µm and 1.0×10^{17} cm^{-3}, in turn. The addition of 0.2 µm of NiO BSF can effectively enhance V_{OC} to ~ 0.1 V. The optimization of p-Si base thickness results a QE ~ 86.83% for the photons wavelength of 1000 nm. The changes in other parameters like working temperature, series and shunt resistances have notable impact on the operations of the device. Therefore, a p-Si wafer based heterojunction arrangement like this could lead to an enhanced efficiency in future solar market.

Acknowledgements The SCAPS simulation program was provided by Dr. Marc Burgelman of the University of Gent in Belgium, for which the authors are very grateful.

Authors' Contributions Nusrat Jahan Konok and Shaikh Khaled Mostaque prepared the original draft, data collection and analysis; Jaker Hossain conceptualized, validated data, supervised and wrote and reviewed the manuscript.

Funding There is no funding to report.

Data Availability No datasets were generated or analysed during the current study.

Declarations

Ethics Approval Not applicable.

Consent to Participate All authors agreed to this submission.

Consent for Publication All authors have read and agreed to the published version of the manuscript.

Competing Interests The authors declare no competing interests.

References

1. Danel A, Chaugier N, Veirman J, Varache R, Albaric M, Pihan E (2022) Closing the gap between n- and p-type silicon heterojunction solar cells: 24.47% efficiency on lightly doped Ga wafers. Prog Photovoltaics Res Appl 31:1235–1244. https://doi.org/10.1002/pip.3635
2. Web: https://chintglobal.com/blog/n-type-vs-p-type-solar-panels/. Accessed 19 Jan 2024
3. Bagher AM, Vahid MMA, Mohsen M (2015) Types of Solar Cells and Application. Am J. Opt Photonics 3. https://doi.org/10.11648/j.ajop.20150305.17
4. Martí A, Araújo GL (1996) Limiting efficiencies for photovoltaic energy conversion in multigap systems. Sol Energy Mater Sol Cells 43:203–222
5. Li W, Buddhiraju S, Fan S (2020) Thermodynamic limits for simultaneous energy harvesting from the hot sun and cold outer space. Light Sci Appl 9:68. https://doi.org/10.1038/s41377-020-0296-x
6. Pandey R, Bhattarai S, Sharma K, Madan J, Al-Mousoi AK, Mohammed MK, Hossain MK (2023) Halide composition engineered a non-toxic perovskite–silicon tandem solar cell with 30.7% conversion efficiency. ACS Appl Electron Mater 5:5303–5315
7. Green MA (2003) Third generation photovoltaics: advanced solar energy conversion. Springer. Berlin. https://doi.org/10.1007/b137807
8. Andreani LC, Bozzola A, Kowalczewski P, Liscidini M, Redorici L (2019) Silicon solar cells: Toward the efficiency limits. Adv Phys X 4:1548305. https://doi.org/10.1080/23746149.2018.1548305
9. Joy A, Abir AT, Mondal BK, Hossain J (2023) Numerical studies on a ternary $AgInTe_2$ chalcopyrite thin film solar cell. Heliyon 9:e19011. https://doi.org/10.1016/j.heliyon.2023.e19011

10. Islam MC, Mondal BK, Ahmed T, Pappu MAH, Mostaque SK, Hossain J (2023) Design of a highly efficient n-CdS/p-AgGaTe$_2$/p$^+$-SnS double-heterojunction thin film solar cell. Eng Res Express 5:025056. https://doi.org/10.1088/2631-8695/acd98a
11. Pappu MAH, Kuddus A, Mondal BK, Abir AT, Hossain AJ (2023) Design of n-CdS/p-CuInTe$_2$/p$^+$-MoS$_2$ thin film solar cell with a power conversion efficiency of 34.32%. Opt. Contin. 2:942–955. https://doi.org/10.1364/OPTCON.486044
12. Battaglia C, Cuevas A, De Wolf S (2016) High-efficiency crystalline silicon solar cells: Status and perspectives. Energy Environ Sci 9:1552. https://doi.org/10.1039/c5ee03380b
13. Hashemi M, Minbashi M, Ghorashi SMB, Abadi A, Ghobadi A, Ehsani MH, Heidariramsheh M, Hajjiah A (2021) Electrical and optical characterization of sprayed In$_2$S$_3$ thin films as an electron transporting layer in high efficient perovskite solar cells. Sol Energy 215:356–366. https://doi.org/10.1016/j.solener.2020.12.046
14. Timoumi A, Bouzouita H, Kanzari M, Rezig B (2005) Fabrication and characterization of In$_2$S$_3$ thin films deposited by thermal evaporation technique. Thin Solid Films 480–481:124–128. https://doi.org/10.1016/j.tsf.2004.11.036
15. Chaudhary M, Doiphode V, Shinde P, Punde A, Vairale P, Hase Y, Waghmare A, Prasad M, Jadkar S (2019) Structural and optical properties of In$_2$S$_3$ thin films deposited by sulfurization assisted thermal evaporation method. Mater Today Proc 39:1889–1993. https://doi.org/10.1016/j.matpr.2020.07.708
16. Cui X, Shi C, Ying C, Wang Q, Sun X, Chen W (2022) The low temperature pyrolysis preparation of In$_2$S$_3$ thin film and its application in Sb$_2$S$_3$ thin film solar cells. Mater Sci Semicond Process 137:106186. https://doi.org/10.1016/J.MSSP.2021.106186
17. Hakim A, Hossain J, Khan KA (2009) Temperature effect on the electrical properties of undoped NiO thin films. Renew Energy 34:2625–2629. https://doi.org/10.1016/j.renene.2009.05.014
18. Napari M, Huq TN, Hoye RLZ, MacManus-Driscoll JL (2021) Nickel oxide thin films grown by chemical deposition techniques: Potential and challenges in next-generation rigid and flexible device applications. InfoMat 3:536–575. https://doi.org/10.1002/inf2.12146
19. Ferdiansjah, Faridah, Mularso KT (2018) Analysis of Back Surface Field (BSF) performance in P-type and N-type monocrystalline silicon wafer. E3S Web Conf. 43:01006. https://doi.org/10.1051/e3sconf/20184301006
20. Fossum JG (1977) Physical operation of back-surface-field silicon solar cells. IEEE Trans Electron Devices 24:322–325. https://doi.org/10.1109/T-ED.1977.18735
21. Xiao D, Dong-Ming W, Xun L, Qiang L, Kai S, De-Zhao W, Ling-Ling W, De-Liang W (2017) Nickel oxide as back surface field buffer layer in CdTe thin film solar cell. Wuli Xuebao/Acta Phys Sin 66:117301. https://doi.org/10.7498/aps.66.117301
22. Xiao D, Li X, Wang D, Li Q, Shen K, Wang D (2017) CdTe thin film solar cell with NiO as a back contact buffer layer. Sol Energy Mater Sol Cells 169:61–67. https://doi.org/10.1016/j.solmat.2017.05.006
23. Medina JCZ, Andres ER, Ruiz CM, Espinosa EC, Yarce LT, Isasmendi RG, Trujillo RR, Salgado GG, Solis AC, Caballero FGN (2023) Numerical simulation and performance optimization of a solar cell based on WO$_3$/CdTe heterostructure using NiO as HTL layer by SCAPS 1D. Coatings 13:1436. https://doi.org/10.3390/coatings13081436
24. Ahmmed S, Aktar A, Hossain J, Ismail ABM (2020) Enhancing the open circuit voltage of the SnS based heterojunction solar cell using NiO HTL. Sol Energy 207:693–702. https://doi.org/10.1016/j.solener.2020.07.003
25. Chen Y, Sun Y, Dai X, Zhang B, Ye Z, Wang M, Wu H (2015) Tunable electrical properties of NiO thin films and p-type thin-film transistors. Thin Solid Films 592:195–199. https://doi.org/10.1016/j.tsf.2015.09.025
26. Muchahary D, Ram LS, Narzary R, Sahu PP, Bhattarai S, Tayal S (2022) Heterojunction between crystalline silicon and nanocomposite coupled ZnO·SnO$_2$ and optimization of its photovoltaic performance. Curr Appl Phys 38:15–21
27. Gogoi M, Bhattarai S, Das TD (2023) A simulation approach for optimization of optical absorption in amorphous silicon solar cell. Mater Today Proc 73:604–607
28. Mostaque SK, Mondal BK, Hossain J (2022) Numerical simulation on the impurity photovoltaic (IPV) effect in c-Si wafer-based dual-heterojunction solar cell. Mater Today Commun 33:104442. https://doi.org/10.1016/J.MTCOMM.2022.104442
29. Hossen MS, Abir AT, Hossain J (2023) Design of an efficient AgInSe$_2$ chalcopyrite-based heterojunction thin-film solar cell. Energy Technol 11:2300223. https://doi.org/10.1002/ente.202300223
30. Zhao Z, Cao Y, Yi J, He X, Ma C, Qiu J (2012) Band-edge electronic structure of β-In$_2$S$_3$: The role of s or p orbitals of atoms at different lattice positions. ChemPhysChem 13. https://doi.org/10.1002/cphc.201100968
31. Koike K, Goto T, Nakamura S, Wada S, Fujii K (2018) Investigation of carrier transfer mechanism of NiO-loaded n-type GaN photoanodic reaction for water oxidation by comparison between band model and optical measurements. MRS Commun 8:480–486. https://doi.org/10.1557/mrc.2018.51
32. Kuddus A, Hossain J, Ismail ABM (2021) Design of a highly efficient CdTe-based dual-heterojunction solar cell with 44% predicted efficiency. Sol Energy 221:488–501. https://doi.org/10.1016/j.solener.2021.04.062
33. Hossain J, Mondal BK, Mostaque SK (2021) Computational investigation on the photovoltaic performance of an efficient GeSe-based dual-heterojunction thin film solar cell. Semicond Sci Technol 37:015008
34. Hossain J, Mondal BK, Mostaque SK (2022) Design of a highly efficient FeS$_2$-based dual-heterojunction thin film solar cell. Int J Green Energy 19:1531–1542. https://doi.org/10.1080/15435075.2021.2011291
35 Mostaque SK, Kumar Mondal B, Hossain J (2022) Theoretical insight into the enhancement of longer-wavelength light absorption in silicon solar cell with multilevel impurities. Results Opt 8:100250. https://doi.org/10.1016/j.rio.2022.100250
36. Verma M, Routray SR, Mishra GP (2020) Analysis and optimization of BSF layer for highly efficient GaInP single junction solar cell. Mater Today Proc 43:3420–3423. https://doi.org/10.1016/j.matpr.2020.09.073
37. Sze SM, Ng KK (2006). Physics of Semiconductor Devices. https://doi.org/10.1002/0470068329
38. Singh P, Ravindra NM (2012) Temperature dependence of solar cell performance - An analysis. Sol Energy Mater Sol Cells 101:36–45. https://doi.org/10.1016/j.solmat.2012.02.019
39. Fan JCC (1986) Theoretical temperature dependence of solar cell parameters. Sol Cells 17:309–315. https://doi.org/10.1016/0379-6787(86)90020-7
40. Web: https://en.wikipedia.org/wiki/Fermi-Dirac_statistics. Accessed 19 Jan 2024
41. Sproul AB, Green MA (1991) Improved value for the silicon intrinsic carrier concentration from 275 to 375 K. J Appl Phys 70:846–854. https://doi.org/10.1063/1.349645
42. Kuddus A, Mostaque SK, Hossain J (2021) Simulating the performance of a high-efficiency SnS-based dual-heterojunction thin film solar cell. Opt Mater Express 11:3812–3826
43. Ahmmed S, Aktar A, Rahman MH, Hossain J, Ismail ABM (2021) Design and simulation of a high-performance CH$_3$NH$_3$Pb(I$_{1-x}$Clx)$_3$-based perovskite solar cell using a CeO$_x$

electron transport layer and NiO hole transport layer. Semicond Sci Technol 36:035002. https://doi.org/10.1088/1361-6641/abd266
44. Bhattacharya S, John S (2019) Beyond 30% conversion efficiency in silicon solar cells: a numerical demonstration. Sci Rep 9:12482. https://doi.org/10.1038/s41598-019-48981-w
45. Nalianya MA, Awino C, Barasa H, Odari V, Gaitho F, Omogo B, Mageto M (2021) Numerical study of lead free CsSn0.5Ge0.5I3 perovskite solar cell by SCAPS-1D. Optik 248:168060
46. Mondal BK, Mostaque SK, Rashid MA, Kuddus A, Shirai H, Hossain J (2021) Effect of CdS and In_3Se_4 BSF layers on the photovoltaic performance of PEDOT:PSS/n-Si solar cells: Simulation based on experimental data. Superlattices Microstruct 152:106853. https://doi.org/10.1016/j.spmi.2021.106853
47. Mondal BK, Mostaque SK, Hossin J (2023) Unraveling the effects of a GeSe BSF layer on the performance of a $CuInSe_2$ thin film solar cell: a computational analysis. Opt Contin 2:428–440
48. Hossain J, Kasahara K, Harada D, Islam ATMS, Ishikawa R, Ueno K, Hanajiri T, Nakajima Y, Fujii Y, Tokuda M, Shirai H (2017) Barium hydroxide hole blocking layer for front- and back-organic/crystalline Si heterojunction solar cells. J Appl Phys 122:055101
49. Procel P, Maccaronio V, Crupi F, Cocorullo G, Zanuccoli M, Magnone P, Fiegna C (2014) Analysis of the impact of doping levels on performance of back contact - back junction solar cells. Energy Procedia 55:128–134. https://doi.org/10.1016/j.egypro.2014.08.095